Electronic Supporting Information

Accessing stable Zirconium Carboxy-aminophosphonate Nanosheets as Support for Highly Active Pd Nanoparticles

Ferdinando Costantino, Riccardo Vivani, Maria Bastianini, Luca Ortolani, Oriana Piermatti, Morena Nocchetti and Luigi Vaccaro**

1. Experimental Section

Synthesis of $Zr_2(PO_4))(L)_2 \cdot H_2O$ (ZPGly). The synthesis of ZPGly was achieved as reported in the reference [14]. In particular, 2.37 g (9 mmol) of N,N-bis(phosphonometyl)glycine (L) were dissolved in 93 ml of deionized water (0.097 M), and then 6 ml of phosphoric acid 1 M were add to this solution. 1.93 g (6 mmol) of $ZrOCl_2 \cdot 8H_2O$ were dissolved in 20.4 ml of HF 2.9 M (59 mmol), molar ratio HF/Zr^{IV}= 10. These two solutions were mixed in a 500 mL Teflon bottle and placed in an oven at 90 °C. After three days the solid was filtered under vacuum, washed three times with deionized water, and dried at 60 °C for 24 h. The empirical formula was $Zr_2P_5O_{21}C_8N_2H_{19}$ (PF= 816, IEC=3.67 mmol/g)

Preparation of ZPGly dispersion. 1g of ZPGly (1.23 mmol) was suspended in 108 ml of deionized water and then 22 ml of n-propylamine 0.1 M (2.2 mmol corresponding to 60% of IEC) were added under vigorous magnetic agitation. A stable dispersion was obtained.

Preparation of Pd@ZPGly composites. 14 ml of $Pd(CH_3COO)_2$ 0.05 M in acetone (0.7 mmol of Pd^{II}) were added drop by drop to 32.5 ml of the ZPGly dispersion (containing 250 mg of ZPGly) under vigorous agitation. The dispersion was left under magnetic agitation for 1 day (Pd@ZPGly-1). Additional composites were obtained by increasing the reaction time to 7 days (Pd@ZPGly-7) and to

15 days (Pd@ZPGly-15). The solids were recovered by ultracentrifugation (15000 rpm for 10 minutes) and washed once with acetone and twice with deionized water. The solids were dried over P_2O_5.

Elemental analysis. Zirconium, phosphorus and palladium contents of samples were obtained by inductively coupled plasma−optical emission spectrophotometry (ICP−OES) using a Varian Liberty Series II instrument working in axial geometry after the mineralization of samples with hydrofluoric acid.

Carbon, nitrogen, and hydrogen content was determined by elemental analysis using an EA 1108 CHN Fisons instrument.

XRPD. XRPD patterns were collected with Cu Kα radiation on a PANalytical X'PERT PRO diffractometer, PW3050 goniometer equipped with an X'Celerator detector. The long fine focus (LFF) ceramic tube operated at 40 kV and 40 mA. To minimize preferential orientations of the microcrystals, the samples were carefully side-loaded onto an aluminum sample holder with an oriented quartz monocrystal underneath.

TEM characterization. TEM investigation was done using a Tecnai F20 TEM microscope, operated at 200 kV accelerating voltage, equipped with STEM high-angle-annular dark-field (HAADF) detector for mass-thickness Z-contrast imaging, and X-rays energy loss spectrometer for elemental mapping (EDX). TEM samples were prepared by drop casting the solution containing the Pd supported ZPGly nanosheets on conventional TEM holey carbon grids.

AFM measurement. Atomic Force Microscope (Solver-Pro, NT-MDT) was also used to provide information on the nanosheet thickness. The measurements were carried out in semicontact conditions by using 190-325 kHz cantilever having a 10 nm radius. The dispersion of zirconium phosphonate exfoliated with propylamine solution was deposited on mica support by spin coating (4000 rpm, 20 s).

FE-SEM characterization. The morphology of ZPGly before and after the exfoliation was investigated by using a FEG LEO 1525 field emission scanning electron microscope (FE-SEM). FE-SEM micrographs were collected after depositing the samples on a stub and sputter coating with chromium for 20 seconds. The ZPGly exfoliated with propylamine solution was freeze dried to obtain a solid to be observed by SEM.

2. Characterization of ZPGly colloidal dispersion

The ability of ZPGly to intercalate basic species, *via* acid-base interaction between the amino group and P-OH or –COOH groups of the layers, was investigated by titrating an aqueous dispersion of ZPGly with a aqueous solution of n-propylamine 0.1 M. The titration curve is reported in Figure S1. After a first burst increase of pH, the pH of the dispersion remains almost constant as the propylamine was added. Finally, an inflection point, where all the acidic protons are neutralized, was reached. The amount of propylamine added was 3.22 mequiv/g, this value is very close to the calculated ion exchange capacity (IEC) of the solid that is 3.67 mequiv/g. The calculate IEC value was obtained considering that the solid contain 3 acidic proton *per* unit formula ((3×1g/816(g/mol))×1000=3.67 mequiv/g).

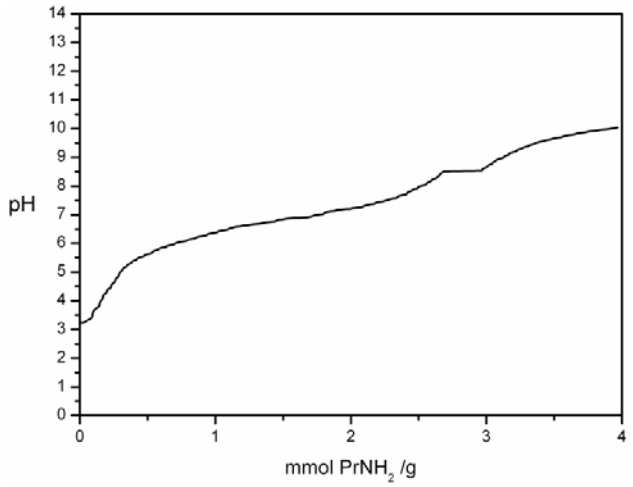

Figure S1. Titration curve of ZPGly with 0.1 M propylamine solution.

The titrated ZPGly was recovered by centrifugation, washed with deionized water, dried over P_2O_5 and analyzed by XRPD. The pattern of ZPGly intercalated with propylamine (ZPGly-$PrNH_2$) (Figure S2-b), compared with those of crystalline ZPGly (Figure S2-a), shows two reflections at low angles: the first at 5.18 2theta (17.0 Å) and the second at 6.97 2theta (14.8 Å) assigned to ZPGly-$PrNH_2$ and ZPGly respectively. The presence of the pristine ZPGly indicated that a little fraction of protons were not involved in the protonation of the propylamina according with lower amount of propylamina added in the titration with respect the calculated IEC (3.22 mequiv/g vs 3.67 mequiv/g).

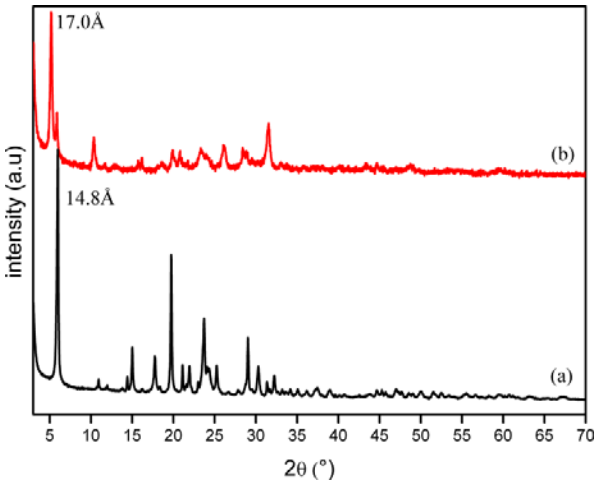

Figure S2. XRPD pattern of (a) ZPGly and (b) ZPGly-$PrNH_2$.

During the titration, it was observed that once the added propylamine reached the 60% of the IEC a colloidal dispersion was obtained. The ability of the solids to give colloidal dispersions is an important feature because it opens the opportunity to intercalate species with high steric hindrance

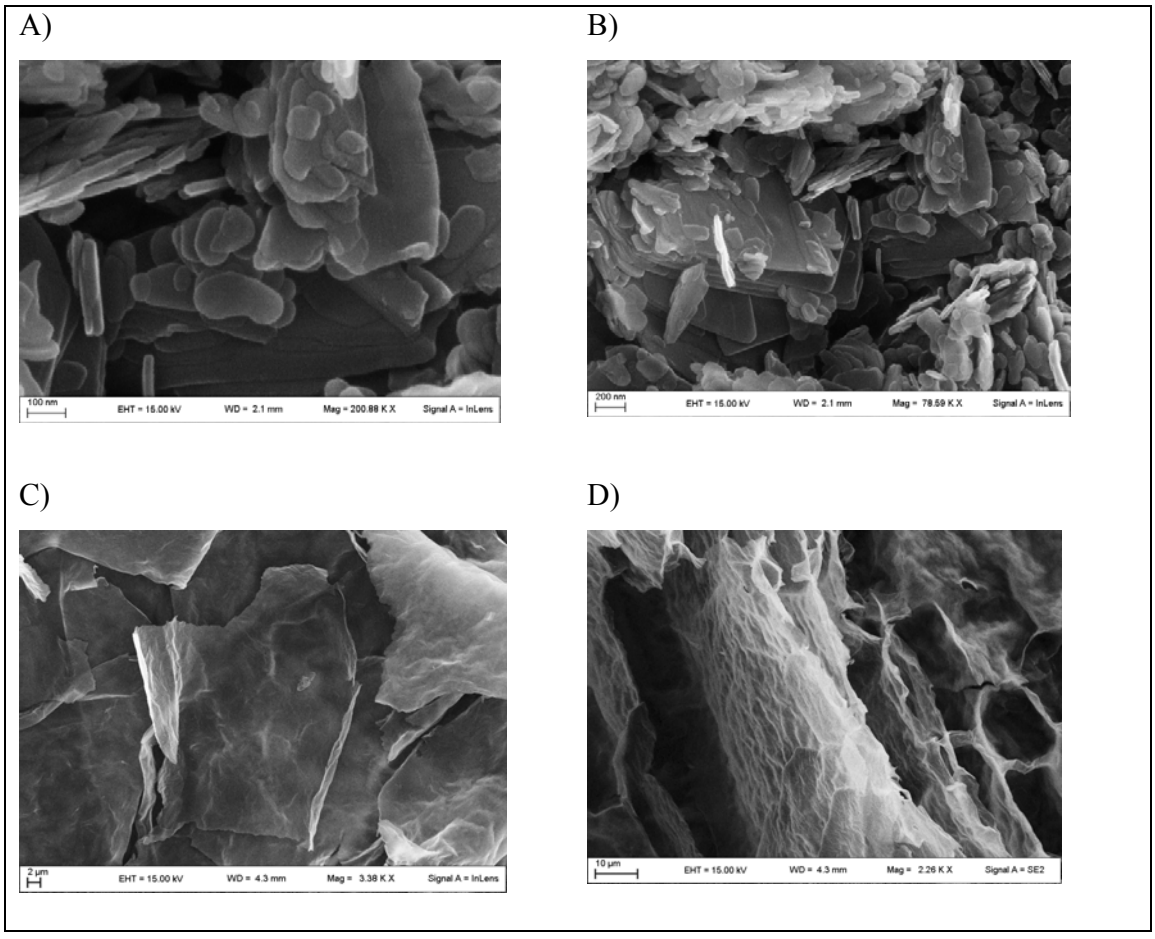

Figure S3. FE-SEM images of ZPGly before (A and B) and after dipersion with propylamine (C and D)

The morphology of ZPGly before and after the exfoliation was investigated by using a FEG LEO 1525 field emission scanning electron microscope (FE-SEM). FE-SEM micrographs were collected after depositing the samples on a stub and sputter coating with chromium for 20 seconds. The ZPGly exfoliated with propylamine solution was freeze dried to obtain a solid to be observed by SEM (Figure S3).

3. Intercalation and characterization of Pd^{II} into ZPGly

In order to intercalate palladium ions into ZPGly a solution 0.05 M of palladium acetate in acetone was added to the ZPGly dispersion. The resulting dispersion was kept under stirring at room temperature for 1, 2, 7 and 15 days and the solids were recovered by ultracentrifugation (hereafter Pd@ZPGly-1, Pd@ZPGly-2, Pd@ZPGly-7, Pd@ZPGly-15) washed with acetone and deionized water and dried over P_2O_5. The XRPD of the samples are reported in Figure S4. Increasing the reaction time, the palladium phase (22.7 Å) turns in ZPGly phase's favour (14.8 Å). Figure S5 reports the relative intensity of Pd@ZPGly phase ($100 \times I_{Pd@ZPGly}/(I_{Pd@ZPGly} + I_{ZPGly})$), that is, in first approximation, correlated to the Pd@ZPGly phase percentage, as a function of the reaction time. In Table S1 are reported Zr, P, Pd, C, N weight percentage determined by elemental analysis and ICP and the Pd/Zr molar ratio of the Pd@ZPGly samples collected after different reaction time. The Pd/Zr molar ratio, except for Pd@ZPGly-1, is equal or higher than those expected (Pd/Zr=0.75), calculated considering that all the exchangeable protons are replaced by Pd^{II}. The excess of palladium, with respect to the negative charges of the layers, can be possible if the palladium is present in it reduced form. In this connection, the increase of ZPGly phase with the reaction time can be explained assuming that during the time a partial reduction of Pd^{II} to metallic Pd occurs and the excess of negative charges of the layers are balanced by protons regenerating the hydrogen phase of zirconium phosphonate. Considering that the pH of the ZPGly dispersion is about 7 the water may be able to reduce palladium ions to metallic palladium.

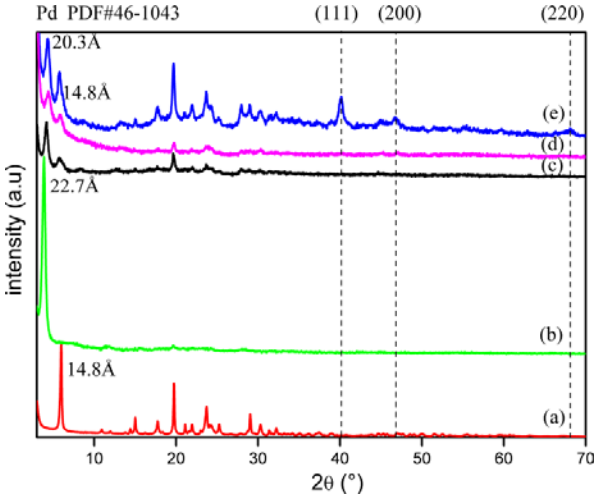

Figure S4. XRPD patterns of (a) crystalline ZPGly, (b) Pd@ZPGly-1, (c) Pd@ZPGly-2, (d) Pd@ZPGly-7 and (d) Pd@ZPGly-15. The dashed lines refer to cubic Pd (PDF#46-1043).

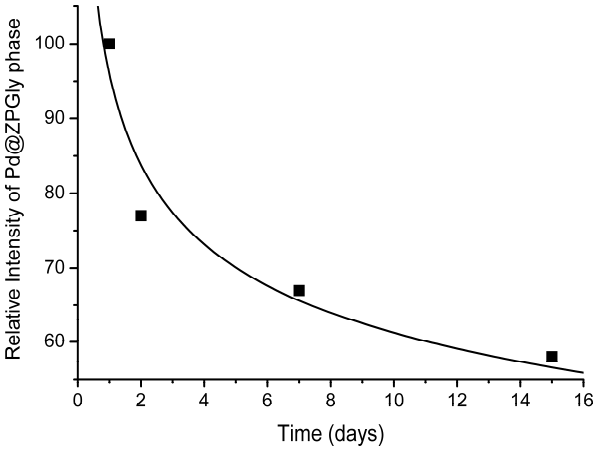

Figure S5. Relative intensity of Pd@ZPGly as function of reaction time.

Table S1. Found weight percentage of Zr, P, Pd, C, N and Pd/Zr molar ratio for ZPGly and Pd@ZPGly collected after 1, 2, 7 and 15 days.

Sample	% w/w					Pd/Zr molar ratio
	Zr	P	Pd	C	N	
ZPGly	23.1	18.5	-	10.4	3.0	-
Pd@ZPGly-1	17.1	11.8	9.8	15.8	5.3	0.50
Pd@ZPGly-2	18.6	14.1	15.9	11.5	3.4	0.73
Pd@ZPGly-7	17.4	11.9	15.1	10.9	3.1	0.74
Pd@ZPGly-15	17.2	13.9	19.3	10.1	2.9	0.96

Figure S6 shows TEM images of Pd@ZPGly after different reaction time. After 1 day the uniform coverage of very small (2 to 5 nm) of Pd NPs can be noticed. As the time increases the number and the size of Pd NPs increases. It is worth to be noted that Pd/Zr ratios increases from 0.50 (after 1 day) to 0.96 (after 15 days) which is about 90% more than the initial value. A population of NPs as large as 20 nm appeared on the sample after 15 days. This suggests that long contacting time favours high Pd loading and the formation of bigger NPs. Notably, the *(111)* and *(200)* peaks of metallic Pd are visible only into the pattern collected after 15 days. For this sample, the Pd NPs diameter was also calculated by applying the Debye-Scherrer equation to the *(111)* and *(200)* Bragg reflections of cubic phase of Pd taking into account the correction for the instrumental line width broadening. The X-ray diffraction pattern was fitted by using a Pseudo-Voigt profile function to obtain the FWHM related to *(111)* and *(200)* peaks (Figure S4). The calculated mean particle size was 18.3 nm in good agreement with the dimension of the bigger population detected by TEM that is 20 nm.

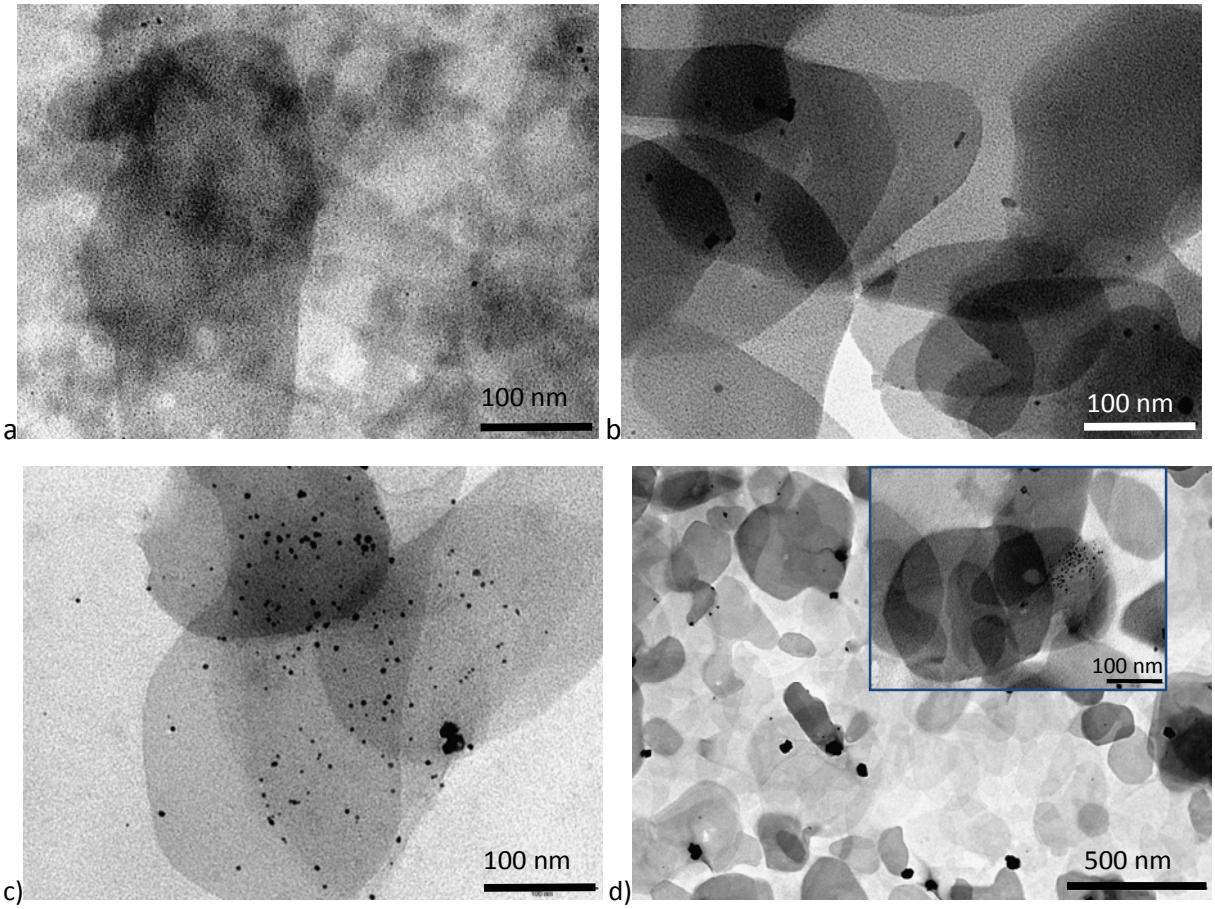

Figure S6. TEM images of Pd@ZPGly after (a) 1, (b) 2, (c) 7 and (d) 15 days of reaction time.

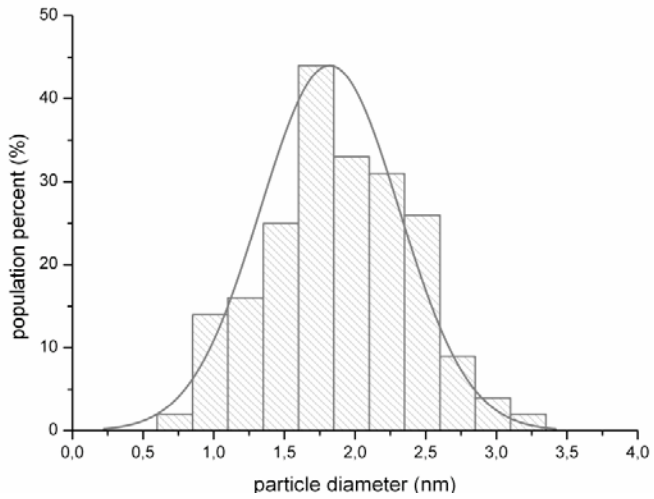

Figure S7. Size distribution and population of the smaller population of Pd nanoparticles on Pd@ZPGly-15.

To highlight the propylamine role the Pd^{II} intercalation into ZPGly was achieved in absence of propylamine. The colloidal dispersion of ZPGly was washed with chloride acid solution at pH=4 in order to remove the propylamine and regenerate the ZPGly in form of a gel. The gel was equilibrated with a solution of $Pd(CH_3COO)_2$ 0.05 M in acetone under vigorous agitation. The dispersion was left under magnetic agitation for 1 day (Pd@HZPGly-1) and for 15 days (Pd@HZPGly-15). The solids were recovered by ultracentrifugation (15000 rpm for 10 minutes) and washed once with acetone and twice with deionized water. The solids were dried over P_2O_5. The XRPD are reported in Figure S8 and no increase of the interlayer distance is detected after the equilibration of ZPGly with palladium acetate solution. However, after 15 days of equilibration the reflections of Pd cubic appear indicating the reduction of the palladium ions. In absence of propylamine the palladium uptake is very low confirming the crucial role of the amine.

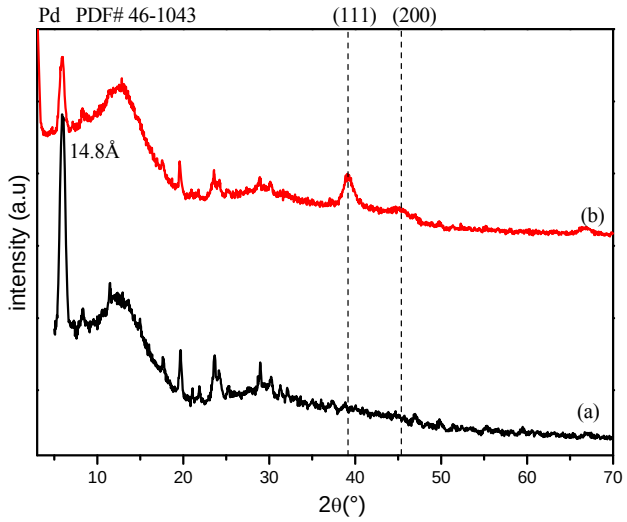

Figure S8. XRPD patterns of (a) Pd@HZPGly-1 and (b) Pd@HZPGly-15. The dashed lines refer to cubic Pd (PDF#46-1043).

4. TEM image of Pd@ZPGly-15 after catalytic runs

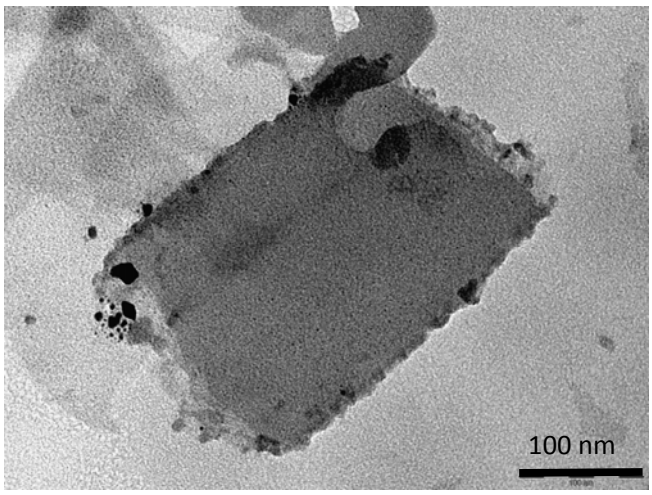

Figure S9. TEM image of Pd@ZPGly-15 after three catalytic runs.

5. Comparative data of catalytic activity

Table S2. Comparison of the efficiency of different Pd-catalytic systems reported by our group.

Reaction of phenylboronic acid (**1**) and 4-bromotoluene (**2a**) under batch conditions

CAT	Medium	T °C	t (h)	Conv. %
Pd@ZPGly-15	EtOH 96%	80	24	98
	$EtOH/H_2O$ (1:1)	80	2	>99
Pd/α-ZrPK[a]	EtOH 96%	80	24	38[b]
	$EtOH/H_2O$ (1:1)	80	2	78[b]

[a] C. Petrucci, M. Cappelletti, O. Piermatti, M. Nocchetti, M. Pica, F. Pizzo, L. Vaccaro, J Mol Catal A: Chemical 2015, 401, 20-27. [b] Data not publisched previously.

Table S3. Comparative literature survey of the Suzuki reaction between phenylboronic acid (**1**) and 4-bromotoluene (**2a**) by different supported Pd nanoparticles catalysts.

Support material used for Pd nanoparticles	Pd (mol%)	Reaction conditions (medium, base, T °C)	t (h)	Yield%	Ref.
Poly(1,2-diamminobenzene), pDAB	0.28	Toluene, K_2CO_3, 90 °C	8	78	1
Magnetic Fe_3O_4/PPy Nanocomposites	1	H_2O, K_2CO_3, 70 °C	10	85	2
DBU-CCG	0.5	EtOH/H_2O (1:1), K_2CO_3, 80 °C	0.5	97[a]	3
Dendrimer on SiO_2/γ-Fe_2O_3	0.02	EtOH/H_2O (1:1), K_3PO_4, 80 °C	24	91	4
poly(NIPAM-co-4-VP) hydrogel	1	H_2O, K_2CO_3, 60°C	5	95	5
Hydrotalcite	2	H_2O/SDS, K_2CO_3, 100 °C	1.5	82	6
sl-GO	0.01	EtOH/H_2O (1:1), K_2CO_3, rt.	3	99[b]	7
SILPP based materials	0.1	EtOH/H_2O (1:1), K_2CO_3, 50°C	19	98	8
Dendrimers	0.1	EtOH/H_2O (1:1), K_3PO_4, 80 °C	15	99	9
Functionalized magnetic nanoparticles	0.2	EtOH/H_2O (1:1), K_2CO_3, 60 °C	4	90	10
Functionalized magnetic nanoparticles	0.2	EtOH 95%, K_2CO_3, 60 °C	8	84	10

[a] Conversion %. [b] 4-bromoanisole.

1. A. Taher, D. Nandi, M. Chodhary, K. Mallick, New J. Chem. 2015, 39, 5589-5596.
2. X. Sun, Y. Zheng, L. Sun, H. Su, C. Qi., Catal. Lett. 2015, 145, 1047-1053.
3. X. Zhang, C. Yu, C. Wang, Z. Wang, J. Qiu, Mat. Research Bull. 2015, 67, 83–86.
4. C. Deraedt, D. Wang, L. Salmon, L. Etienne, C. Labrugère, J. Ruiz, D. Astruct, ChemCatChem 2015, 7, 303-308.
5. Y. Lee, M. C. Hong, H. Ahn, J. Yu, H. Rhee, J. Organomet. Chem. 2014, 769, 80-93.
6. M.I. Burrueco, M. Mora, C. Jiménez-Sanchidrián, J.R. Ruiz, Appl. Catal. A: General 2014, 485, 196-201.
7. S. Yamamoto, H. Kinoshita, H. hshimoto, Y. Nishina, Nanoscale 2014, 6, 6501-6505.
8. C. Pavia, E. Ballerini, L. A. Bivona, F. Giacalone, C. Aprile, L. Vaccaro, M. Gruttadauria, Adv. Synt. Catal. 2013, 355, 2007-2018.
9. C. Deraedt, L. Salmon, L. Etienne, J. Ruiz. D. Astruct, Chem. Commun. 2013, 49, 8169.
10. Q. Zhang, H. Su, J. Luo, Y. Wei, Catal. Sci. Technol. 2013, 235-243.